



Effect of Alumina on Calcium Ferrites Development in the Goethite Ore Sinters

Dali Hariswijaya¹ · Leonardo Tomas Da Rocha¹ · Edson Kugara Chiwandika¹ · Sung-Mo Jung¹

Received: 14 August 2021 / Accepted: 28 November 2021 / Published online: 16 January 2022
© The Minerals, Metals & Materials Society 2021

Abstract

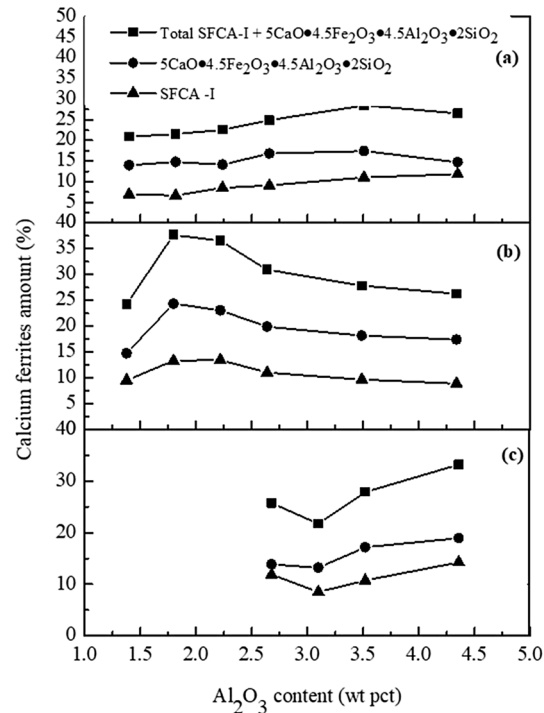
As one of the most common constituent of gangue in iron ore, it has been known that alumina plays an important role in the formation of silico ferrite of calcium aluminum (SFCA), which are derivatives of calcium ferrites. SFCA is the most desirable bonding phase in iron ore sinter due to its high reducibility and mechanical strength. Alumina has been known to promote the formation of SFCA in the sintering process of iron ore, but it also increases the porosity of sintered ore and viscosity of primary melt, and decreased the physical properties of the sintered ore. In order to achieve better understanding about the effect of alumina on sintered iron ore, three kinds of powdered iron ores were investigated under similar condition of identical alumina source and content. The iron ores used in the experiments were Carajas, Yandi, and Australian Premium Iron (API) ores. The formation temperature of primary melt, phase composition, and porosity of each sintered iron ore were measured to find out how they are related. Results showed that the estimated temperature of initial primary melt formation decreased with the addition of small amount of alumina then increased with the further addition of alumina in Yandi ore while in Carajas and API ores, the initial primary melt formation temperature was always increasing with alumina addition. More amount of calcium ferrites were formed in the Yandi and API ores sinter than in the Carajas ore sinter, which showed that the Yandi and API ores have better reactivity since they are goethite-based ores. It was concluded that the amount of calcium ferrites generated and porosity were competing factors that may govern the physical properties of sintered iron ores.

The contributing editor for this article was Il Sohn.

✉ Sung-Mo Jung
smjung@postech.ac.kr

¹ Graduate Institute of Ferrous and Energy Materials
Technology, Pohang University of Science and Technology,
Pohang 37673, Korea

Graphical Abstract



Keywords Iron ore, Sintering · Alumina · SFCA · Phase composition · Porosity

Abbreviations

SFCA	Silico-ferrite of calcium and aluminum
RDI	Reduction degradation index
LOI	Loss on ignition
TI	Tumbler index
API	Australian premium iron

Introduction

Starting from the 21st century, the production of iron ore in the world continues to increase exponentially to satisfy the needs for crude steel production [1], but there is only limited amount of high-grade iron ore deposits available. Thus, it is necessary to utilize low-grade iron ores previously not utilized in blast furnace process to fulfill the requirement of iron ore intake, this includes iron ores containing higher than 2 wt pct of alumina. Alumina has been known to strongly deteriorate tumbler index (TI) and reduction degradation index (RDI) of iron ore sinter [2, 3]. However, other studies showed that the detrimental effects of alumina were not as strong as expected [4]. Newer studies even showed that alumina has various effects on sintered iron ore based on the type of iron ores used in the sinter [4]. These conflicting results possibly occurred because each of those researches

used different kinds of iron ores and alumina sources in their experiments as well as different experimental conditions. In order to properly investigate the effect of alumina on sintered iron ores, it is necessary to conduct the experiments on a variety of iron ores under similar experimental condition of identical source of alumina.

Alumina has been known to strongly affect the formation of silico ferrite of calcium and aluminum (SFCA) during sintering process of iron ore [5]. When alumina reacted with calcium ferrite, calcium iron aluminum oxide formed and acts as a precursor in the formation of SFCA [6]. With development of technology for the phase analyses, it was found that there are two kinds of SFCAs, namely SFCA-I and SFCA [5]. Further studies about these two SFCAs showed that SFCA-I has better physical properties and reducibility compared to SFCA [5]. However, SFCA-I is a metastable phase, which will break into SFCA with longer heating and sintering time [7].

Studies in the first decade of 21st century revealed several effects of alumina on liquid phase formation during sintering process. It was reported that limited amount of alumina will enlarge liquid phase field of sintered iron ore [2], will lower softening temperature [8] but above a certain addition level alumina will increase viscosity of the liquid phase [9], lowers its melt penetration behavior [10], and increases porosity

and pore size in the resulting sinter [11]. Almost all previous studies about the effect of alumina on phase development of sintered iron ore have showed that alumina could promote the formation of calcium ferrite phases, especially SFCA-I and SFCA [3, 4, 12]. As for the effect of alumina on the formation of hematite and magnetite phases, several different results have been reported, a few studies reported that alumina promotes the formation of secondary hematite resulting in higher amount of hematite phase, but lower amount of magnetite phase [3], meanwhile other studies reported that higher alumina content in the sinter mix will form less amount of hematite and magnetite in the resulting sinter [12, 13], which can be attributed to the difference in the chemical composition of the ores used. It has also been reported that the addition of alumina will increase the hardness of each phase in the sintered ore [14] and this includes hematite, magnetite, and SFCA, although the hardening effect of alumina on SFCA phase is much weaker compared to hematite and magnetite phases. Hardened phases generally produce more brittle sinter matrix, which is undesirable.

Alumina in iron ore naturally exists either in the form of kaolinite ($\text{Al}_2\text{O}_3 \cdot 2\text{SiO}_2 \cdot 2\text{H}_2\text{O}$) or gibbsite ($\text{Al}_2\text{O}_3 \cdot 3\text{H}_2\text{O}$). Since kaolinite is distinct from gibbsite, either of them may have different effects on sintered iron ore. It has been reported that higher reactivity of alumina source will produce higher amount of SFCA phases [15, 16], and recently it was found that different reactivity of alumina source will produce SFCA with distinct morphologies [16].

The current research aims to systematically investigate the effects of alumina on sintered iron ore. All of the experiments were carried out with addition of pure alumina as the alumina source. The general understanding about the effect of alumina on sintered iron ore will make it easier to find out the methods of mitigating its harmful effects on sintered iron ore, and then iron ores containing high amount of alumina can be utilized in the iron and steel industry.

Experimental

Materials Preparation

Three kinds of iron ores such as Carajas ore, Yandi ore, and Australian Premium Iron (API) ore were used in the experiments. Carajas ore is one of high-grade hematite ores, which are widely used in the blast furnace operation. Yandi ore is a goethite ore with Al_2O_3 content almost similar to Carajas ore. API ore is a goethite ore of high Al_2O_3 content. Most of the alumina exist as kaolinite [$\text{Al}_2\text{O}_3 \cdot \text{SiO}_2 \cdot 2\text{H}_2\text{O}$] in the Carajas ore, as gibbsite [$\text{Al}(\text{OH})_3$] in the Yandi ore, and as $\text{Fe}_{0.93}\text{Al}_{0.07}\text{O}(\text{OH})$ and gibbsite [$\text{Al}(\text{OH})_3$] in the API ore. The XRD results of the ores are shown in Fig. 1.

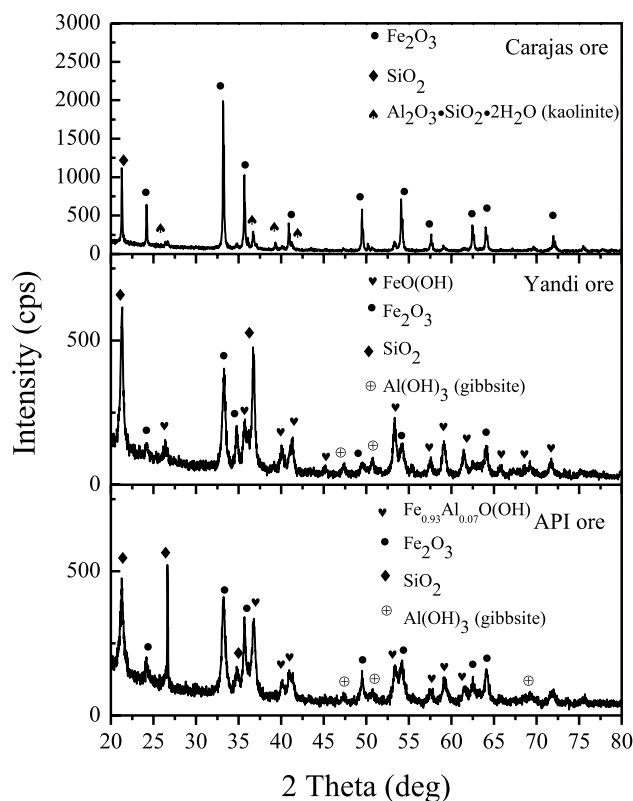


Fig. 1 XRD results of the ores used in the current study

Reagent-grade chemicals of CaO and SiO_2 were used as flux in the experiments to control basicity (CaO/SiO_2), while reagent grade Al_2O_3 was used to increase alumina content of the sinter mixes. All of the ores and reagents were dried at 100°C for 24 h before mixing. Chemical analysis results of the iron ores and reagents are shown in Table 1. The samples were crushed and sieved to a particle size below $250\ \mu\text{m}$ to ensure uniform mixing. However, it should be noted that ores with large particles are used in the actual sintering process.

The synthetic ore was used to make sinter mix by adding CaO , SiO_2 , and Al_2O_3 fluxes, while in the natural ores SiO_2 and CaO were added to adjust SiO_2 content to be above 4 wt pct and basicity (CaO/SiO_2) of all sinter mixes to be maintained at 1.87. The Al_2O_3 content in the sinter mixes prepared from each iron ore ranges from 1.4 to 4.4 wt pct. The chemical composition of sinter mix made from Carajas ore was calculated as shown in Table 2, while that made from Yandi ore is shown in Table 3, and that made from API ore is shown in Table 4.

Since calcium ferrite is considered to be the most important phase in sintered iron ore with a melting temperature of around 1200°C , the primary melt formation temperature in iron ore mix was estimated using thermogravimetric-differential scanning calorimetry (TG-DSC) (TG-DSC 1 Star

Table 1 Chemical composition of iron ores and reagents used (weight percent)

Material	Ore Type	T.Fe	FeO	Fe ³⁺	SiO ₂	Al ₂ O ₃	P ₂ O ₅	CaO	MgO	LOI
Carajas ore	Hematite	65.20	0.17	65.00	2.23	1.63	0.21	0.21	0.14	2.47
Yandi ore	Goethite	56.20	0.80	55.50	6.55	1.61	0.10	0.10	0.09	10.70
API ore	Goethite	57.10	0.20	56.90	5.35	3.14	0.14	0.14	0.05	8.87
Fe ₂ O ₃ reagent	Reagent	69.70	0.24	69.46						
CaO reagent	Reagent							92.20		
SiO ₂ reagent	Reagent				98.00					
Al ₂ O ₃ reagent	Reagent					99.99				

system, Mettler Toledo). Since, melting is an endothermic process, a trough at around 1200 °C in the DSC curve might represent melting of these calcium ferrites.

Experimental Apparatus and Procedure

Initially, the sinter mixes consisting of iron ores and the reagents were analyzed using the TG-DSC to investigate the melting temperature of calcium ferrite in each mix. About 100 mg sample of each mix was heated at a rate of 10 °C/min up to 1400 °C in an Ar atmosphere. The sinter mix prepared by reagent grade Fe₂O₃, Al₂O₃, CaO, and SiO₂ was analyzed to act as the reference sample for the estimation of the primary melt formation temperature. The chemical composition of each reagent mix was calculated as shown in Table 5.

The sintering experiments were done using the horizontal tube furnace. All of the sinter mixes were pressed into discs weighing 1 g, which were then sintered in a horizontal tube furnace in air. The schematic diagram of the experimental apparatus is shown in Fig. 2.

During the sintering process, about 30 discs weighing 1 g each were preheated at a rate of 20 °C/min to 1150 °C in an Ar atmosphere. The low heating rate used in the pre-heating stage was used in order to minimize temperature gradient within the pellets. The assumption was when the temperature reached the target temperature of 1150 °C, the entire pellet was at that temperature to maximize on the formation of bonding phase. After reaching a target temperature of 1150 °C, air was blown to allow for the burning of carbon inside the pellets while the furnace temperature was held at 1150 °C for 1 h. The temperature inside the sample holder was increased to 1280 °C due to the burning of carbon inside the pellets. All the samples took approximately 2.5–3.0 min to reach the maximum temperature of around 1280 °C. Yandi sinter mix took the longest time to reach the maximum temperature followed by API sinter mix and lastly Carajas sinter mix. This might have been attributed to the water content of the ores used to make the sinter mixes as can be seen by the measured loss on ignition (LOI) in Table 1. The final temperature after holding the pellet at 1150 °C for 1 h was about 1165 °C. The furnace was then allowed to naturally cool to room temperature and the sintered pellets were taken out for further investigations. The holding time used in this experiment was much longer than that used in actual sintering to allow for the maximum formation of bonding phases, enabling identification of these phases by XRD [17].

Hsieh et al. [18] reported that in industrial iron ore sintering, the raw materials are heated in low oxygen partial pressure and cooled at high oxygen partial pressure. They designed a range of oxygen partial pressures for simulating the sintering process in the lab. This means that the

Table 2 Composition of sinter mix prepared from Carajas Ore (weight percent)

Component	Mix 1	Mix 2	Mix 3	Mix 4	Mix 5	Mix 6
Fe ₂ O ₃	79.76	79.35	78.95	78.54	77.73	76.92
Al ₂ O ₃	1.40	1.82	2.24	2.66	3.51	4.35
CaO	7.92	7.91	7.91	7.91	7.91	7.91
SiO ₂	4.24	4.24	4.24	4.24	4.24	4.24
C	4.03	4.03	4.03	4.03	4.03	4.03
Other gangue	2.65	2.64	2.62	2.61	2.58	2.56

Table 3 Composition of sinter mix prepared from Yandi Ore (weight percent)

Component	Mix 1	Mix 2	Mix 3	Mix 4	Mix 5	Mix 6
Fe ₂ O ₃	67.88	67.57	67.27	66.96	66.35	65.74
Al ₂ O ₃	1.38	1.80	2.22	2.64	3.49	4.34
CaO	10.49	10.44	10.40	10.35	10.26	10.16
SiO ₂	5.60	5.58	5.55	5.53	5.48	5.43
C	4.02	4.02	4.03	4.03	4.03	4.04
Other gangue	10.63	10.59	10.54	10.49	10.39	10.30

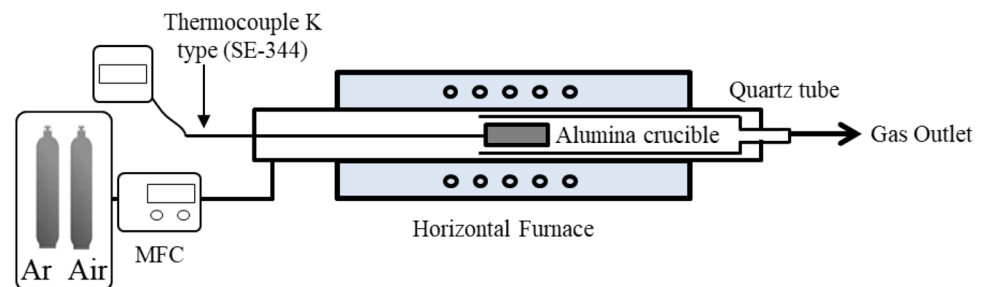
Table 4 Composition of sinter mix prepared from API Ore (weight percent)

Component	Mix 1	Mix 2	Mix 3	Mix 4
Fe ₂ O ₃	77.14	76.70	76.43	75.75
Al ₂ O ₃	2.68	3.10	3.52	4.36
CaO	9.08	9.04	9.00	8.92
SiO ₂	4.85	4.83	4.81	4.76
C	4.04	4.04	4.05	4.03
Other gangue	2.21	2.20	2.19	2.17

exact gaseous atmosphere in real sinter is not known as partial oxygen pressure varies with the burning of coal. In an attempt to simulate the actual sintering process, various partial oxygen pressures as well as various temperatures are normally used for the simulation of different sinter zones. In this experiment, air was opened after attaining the target temperature to allow for the burning of carbon [17]. This ensured that the pellets were exposed to a range of partial oxygen pressures during the sintering. The partial oxygen pressure ranged from low during the burning of carbon to high during cooling in air. The

Table 5 Calculated composition of reagent mix (weight percent)

Component	Mix 1	Mix 2	Mix 3	Mix 4	Mix 5	Mix 6	Mix 7
Fe ₂ O ₃	79.78	78.8	77.81	76.83	75.84	74.86	69.93
Al ₂ O ₃	0	0.98	1.97	2.95	3.94	4.92	9.85
CaO	9.85	9.85	9.85	9.85	9.85	9.85	9.85
SiO ₂	4.925	4.925	4.925	4.925	4.925	4.925	4.925
C	3.94	3.94	3.94	3.94	3.94	3.94	3.94

Fig. 2 Schematic diagram of sintering apparatus

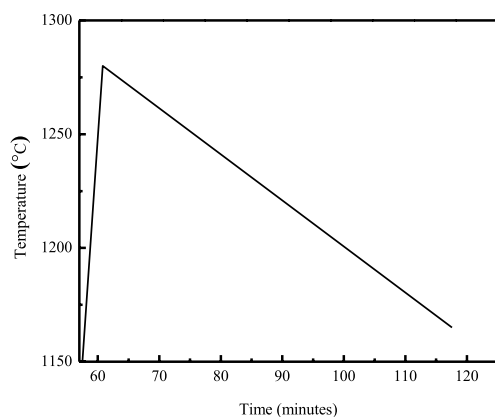


Fig. 3 Representative temperature profile after opening air for the burning of carbon inside pellet

phase identified after sintering was expected to be the major bonding phase in such conditions. Comparison of the phases formed with those reported in literature [5, 19, 20] was done.

The representative temperature profile after opening of air to allow for the burning of carbon is as shown in Fig. 3.

The diameter of each sintered pellet after sintering was measured to be 8.5 mm. About 1 g of the sample was mounted, and polished for observation employing the Scanning Electron Microscopy (SEM, JEOL-(Japan)/JSM-7100F) and Electron Probe Microanalysis (EPMA, JOEL JXA-8530F) at an acceleration voltage of 20 keV. In addition, 1 g was crushed for XRD (Bruker AXS) analysis, and 1 g was used in porosity analysis. In investigating the phases formed in the sintered ores, the sintered samples were analyzed by X-ray diffraction (XRD) Bruker AXS with a Cu tube at a scan angle of 20° to 80°, a rate of 2°/min, sampling 0.02° at a voltage of 40 kV, and current of 40 mA.

The RDI test was carried out using lab scale test for comparison purposes. Pellets were pre-reduced in the horizontal tube furnace by preheating the sample in N₂ atmosphere to 500 °C. The samples were then held for 1 h in 30 vol pct CO and 70 vol pct N₂ atmosphere at 500 °C to allow for reduction and finally the sample was naturally cooled in N₂ atmosphere. Tumbler index and RDI tests were carried out using a lab scale tumbling test apparatus (Universal ball mill (JISICO J-BMM)). About 10 × 1 g discs were used for each tumbler and RDI tests inside a steel cylinder (5 cm ID × 13.5 cm Height). Sintered discs were used for the tumbler test where all of the samples were revolved for 200 revolutions, while pre-reduced discs were used for RDI test where all of the samples were revolved for 200, 400, and 800 revolutions.

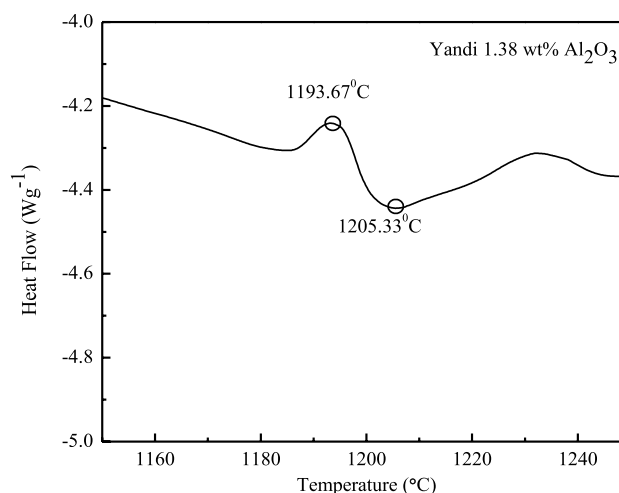


Fig. 4 Typical DSC curve of Yandi Mix 1

Results and Discussion

Estimation of Melting Temperature of Calcium Ferrites

Among all of the phases in the matrix of a sintered ore, calcium ferrite is one of the most common phases found in the matrix, and is an intermediate phase for the formation of SFCA. That is, it is one of the phases greatly affecting the quality of sintered iron ore. In the current experiments, 100 mg of each sinter mix including the synthetic reagents was analyzed using TG-DSC to investigate the effect of increasing alumina content on melting temperature of calcium ferrite in each sample. The formation temperature of primary melt was estimated by the heat flow in the DSC curve of the sinter mix since the primary melt formed in sinter is likely to be composed of the calcium ferrite with a melting temperature of around 1200 °C [17]. Because melting is an endothermic process, a trough in the DSC curve at around 1200 °C was considered to be the formation temperature of primary melt in the sinter mix, as shown in the typical DSC curve for Yandi ore in Fig. 4.

From the DSC curve, the start temperature of primary melt formation (T_m start) was estimated to be 1194 °C, while its finish temperature (T_m finish) was considered to be 1205 °C. The trends in synthetic reagents, Carajas ore mix, Yandi ore mix, and API ore mix are shown in Fig. 5.

When alumina content is lower than 2 wt pct, it is expected that the addition of small amount of alumina would decrease the melting temperature of calcium ferrite due to the presence of eutectic point between calcium ferrite and calcium iron aluminum oxide [21]. Further addition of alumina above 2 wt pct will inhibit the melting, and subsequently increase the melting temperature of calcium ferrite due to the presence of solid calcium iron aluminum

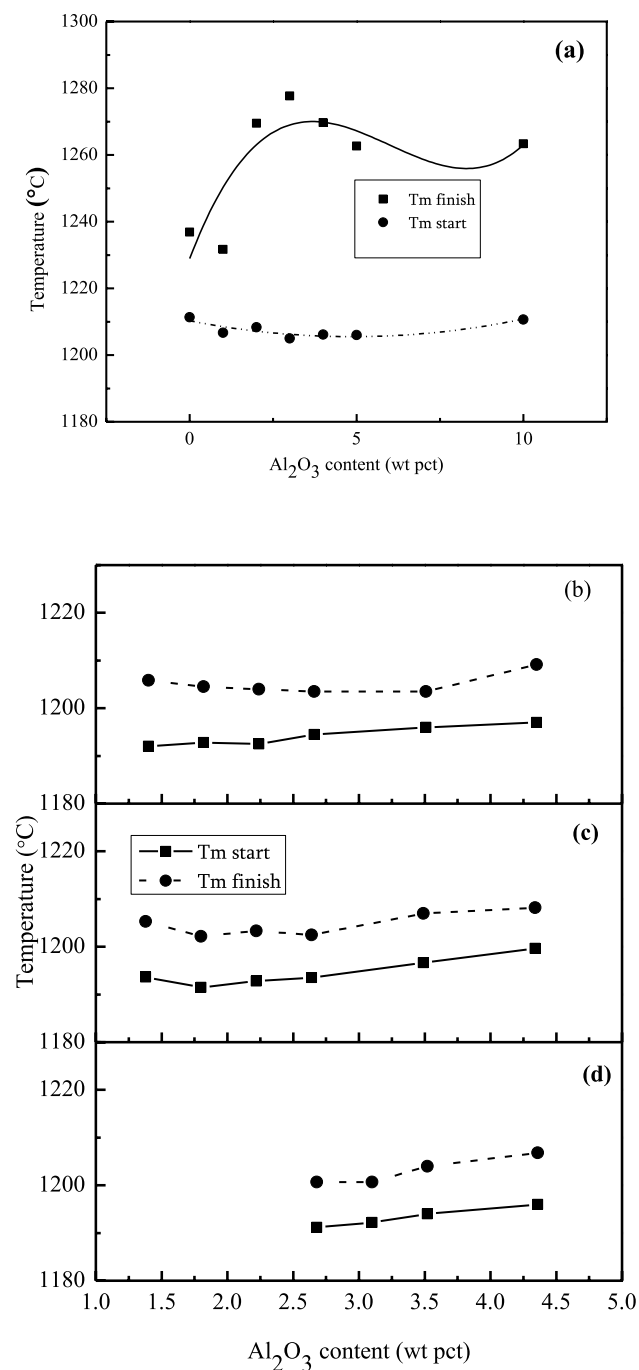


Fig. 5 Estimated temperature of melt formation with increasing alumina content of **a** Synthetic sinter mix, **b** Carajas sinter mix, **c** Yandi sinter mix, and **d** API sinter mix

oxide of high melting temperature [21]. This particular trend was observed on Fig. 5c. In Fig. 5b and d, the initial melt formation temperature was increasing with the addition of alumina. As for the samples prepared from hematite reagents, no particular trend was observed with the increase in alumina content. In all the samples, calcium ferrite starts to melt at approximately 1190 °C. In addition, when

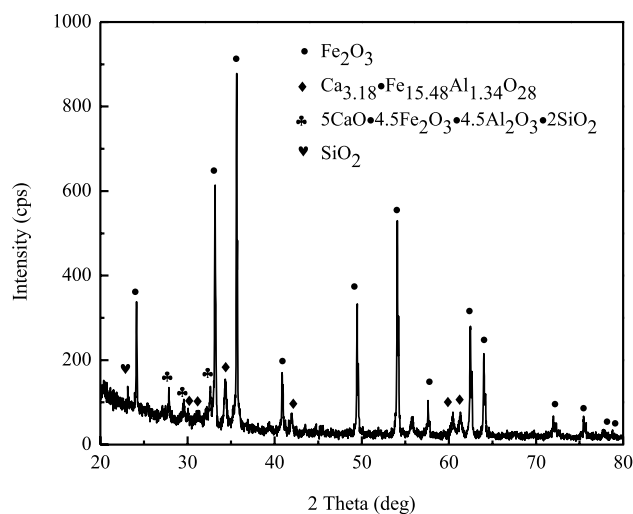


Fig. 6 XRD result of sintered Yandi mix 1

considering the carbon content in sinter mix, it was decided that the sintering process for the subsequent experiments would be started at 1150 °C to preserve as much calcium ferrites as possible.

Phase Composition Evaluated by XRD in Sintered Ore

The peaks identified by XRD were then quantified by calculating the integral value of each subsequent phase peak using Origin Pro software. To ensure accuracy, the analyses were repeated at least 3 times and the average was used as the representative quantity of the calcium ferrite phases in the sintered samples. Based on the XRD database, SFCA-I phases were analyzed as $\text{Ca}_{3.18}\text{Fe}_{15.48}\text{Al}_{1.34}\text{O}_{28}$ (ICDD 00-052-1258) since SFCA-I has a general formula of $\text{M}_{20}\text{O}_{28}$ with low Si in their crystal structure (where $M = \text{Fe}, \text{Ca}, \text{Si}, \text{and Al}$) [5]. $5\text{CaO} \cdot 4.5\text{Fe}_2\text{O}_3 \cdot 4.5\text{Al}_2\text{O}_3 \cdot 2\text{SiO}_2(s)$ (ICDD 00-033-0250) was one of the derivative of calcium ferrite identified in the sintered samples. For example, the XRD result of the sintered Yandi mix 1 is shown in Fig. 6.

In all of the sintered ores, SFCA-I, $5\text{CaO} \cdot 4.5\text{Fe}_2\text{O}_3 \cdot 4.5\text{Al}_2\text{O}_3 \cdot 2\text{SiO}_2(s)$, hematite, and SiO_2 were identified to be the main phases. The quantified calcium ferrite amount from XRD results for sintered Carajas mix, Yandi mix, and API mix are shown in Figs. 7a–c, respectively.

From the analysis of melting temperature of calcium ferrites, it could be expected that the amount of calcium ferrite phases in Yandi mix would increase with the increase in alumina content, and then decrease with the further addition of alumina. This trend was observed in the XRD quantification of sintered Yandi ore as shown in Fig. 7b. Meanwhile, the XRD quantification of Carajas and API ores shown in Fig. 7a and c indicated that the amount of calcium ferrite

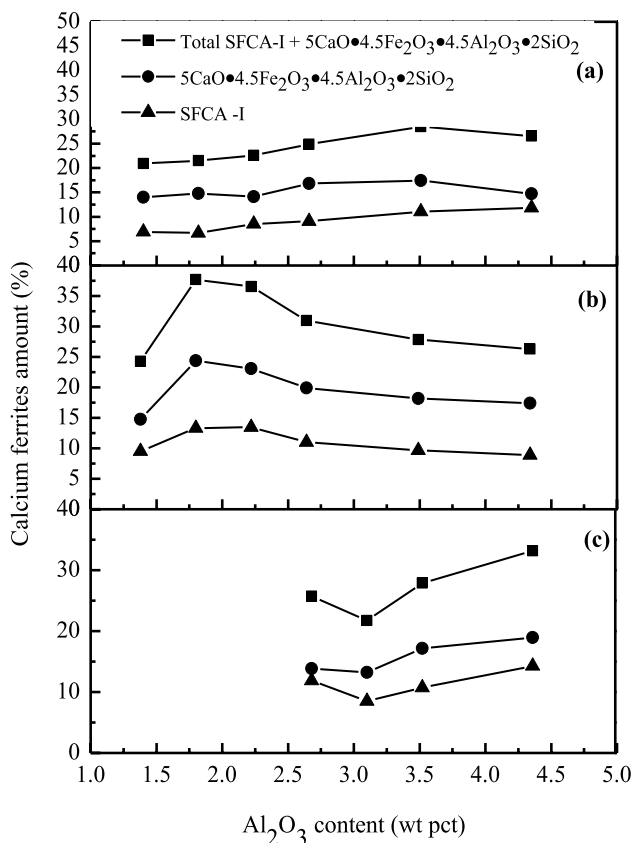


Fig. 7 Change in amounts of calcium ferrite phase composition of: **a** sintered Carajas mix, **b** sintered Yandi mix, and **c** sintered API mix with the increase in alumina content

phases increased with the increase in alumina content. Yandi and API ores are goethite-based, and tend to form high amount of pores during the sintering process, which might result in the increased reactivity of the ores. High reactivity of the goethite ore can be observed from the higher amount of calcium ferrites phases formed compared to sintered Carajas ore.

To verify some of the phases identified by XRD, point analysis by Energy Dispersive X-ray Microscopy (EDS) was done on the mounted and polished sample. The EDS analysis result of the Yandi ore is shown in Fig. 8 and Tables 6 and 7 as an example. In calculating the atomic weight percentage at each point, the carbon content was ignored except for point 3 in Table 7 that mainly consisted of residual carbon.

Figure 8a and Table 6 showed that there were two types of SFCA: one with high amount of Fe and low amounts of Si and the other with low amounts of Fe and high amounts of Si which was in agreement with the XRD results that showed the possibility of the presence of $\text{Ca}_{3.18}\text{Fe}_{15.48}\text{Al}_{1.34}\text{O}_{28}$ (ICDD 00-052-1258) and $5\text{CaO}\cdot 4.5\text{Fe}_2\text{O}_3\cdot 4.5\text{Al}_2\text{O}_3\cdot 2\text{SiO}_2(s)$ (ICDD 00-033-0250). Increasing the alumina content in the Yandi ore showed that the amount of alumina in the SFCA

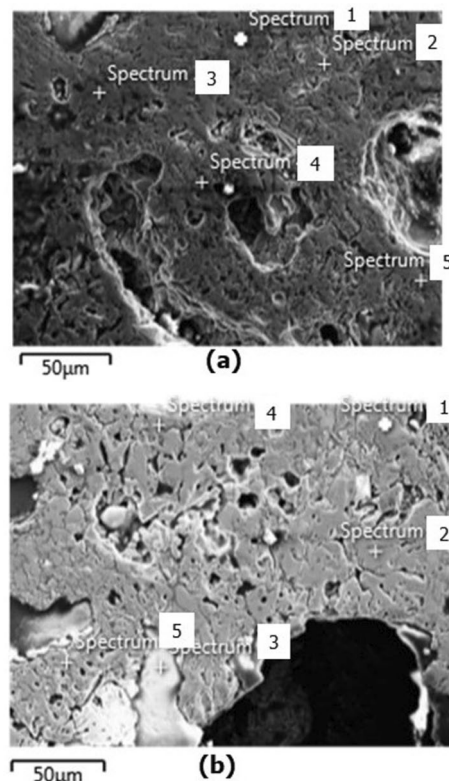


Fig. 8 EDS point analysis of Yandi ore: **a** 1.80 alumina and **b** 3.49 alumina content (Wt Pct)

increased as shown by Fig. 8b and point 4 in Table 7. Figure 7 showed that the amount of calcium ferrites in the sintered Yandi mix with alumina levels of 3.49 wt pct decreased while EDS showed the possibility of the presence of other phases that might include hematite as shown by point 2 and 5 in Table 7. The hematite phase had low amounts of Al and Si in the crystal structure. EPMA mappings were done to provide further evidence.

Elemental Distribution in Sintered Ores

According to the previous studies, it could be expected that the addition of a sufficient amount of alumina in the sintered ore will form massive SFCA structure in the matrix. To confirm location of Al in the sintered ores, the elemental distribution of each sintered ore was obtained by EPMA mappings. Since alumina joins the reactions of sintered ore when they form calcium iron aluminum oxide as a precursor in SFCA formation [6], distribution of aluminum at low concentration in the same area as the Fe-enriched phase might show the existence of either calcium iron aluminum oxide or SFCA. The elemental distribution of sintered Carajas mix, Yandi mix, and API mix are shown in Figs. 9, 10, and 11, respectively.

Table 6 Atomic composition of sintered Yandi ore with 1.80 wt pct alumina (atomic percent)

Position	Elemental content (atomic Pct)				
	Fe	Ca	Al	Si	O
1	17.61	5.71	0.55	20.61	55.52
2	22.33	6.10	1.06	3.34	67.15
3	15.49	4.78	1.05	15.52	63.06
4	12.30	3.52	1.26	12.09	70.82
5	25.51	4.84	1.67	3.10	64.88

Table 7 Atomic composition of sintered Yandi ore with 3.49 wt pct alumina (atomic percent)

Position	Elemental content (atomic Pct)					
	Fe	Ca	Al	Si	O	C
1	37.43	0.15	0.61	0.33	61.48	–
2	34.18	–	0.38	0.48	64.97	–
3	0.65	–	–	0.376	–	98.97
4	28.18	8.90	2.94	4.51	55.47	–
5	39.74	–	0.87	0.26	59.12	–

From Figs. 9 and 11, it can be observed that large amount of Fe, Al, Ca, and Si were distributed in the identical areas starting from above and around 2.6 wt pct of alumina content for the sintered mixes made from Carajas and API ores as shown in Figs. 9d and 11a. This observation could indicate that massive SFCA were formed as supported by the quantified phase composition by XRD in Fig. 7a and c. However, it should be noted that alumina content of 2.68 wt pct was the basic composition for sintered API ore. Meanwhile, it can be observed in Fig. 10 that for sintered mixes made from Yandi ore, massive SFCA starts to form at 1.8 wt pct of alumina content, as can be seen by the areas where Ca, Fe, Al, and Si are highly distributed together. Massive SFCA might start to form at lower alumina content in sintered Yandi ore due to its superior reactivity in contrast to sintered hematite ore. After the formation of massive SFCA, the addition of further alumina showed different results for each iron ore. As observed in Fig. 9 for sintered Carajas ore, the addition of alumina increases the amount of SFCA phase, and forms alumina residue of high concentration as shown by the areas marked in red circle in Figs. 9b–f. Meanwhile, as observed in Fig. 10b for sintered Yandi mix, the addition of further alumina only increases alumina concentration in the SFCA matrix, this may explain the decreasing trend of SFCA phase in sintered Yandi ore with the increase in alumina addition after a significant increase at 1.80 wt pct of alumina content, which is shown by the XRD quantified results in Fig. 7b and the EDS result in Fig. 8a and b and Table 6 and 7. It seems that the addition of further alumina to Yandi ore made the excess of alumina to diffuse into existing SFCA phases instead of forming new SFCA phases, this promoted the decomposition of SFCA phases into hematite shown in Table 7 and some other phases. Sintered API mixes showed

intermediate behavior between sintered Carajas mix and sintered Yandi mix where the amount of SFCA was increased, but the alumina concentration in SFCA matrix also increases as shown in Fig. 11a–d.

Pore Development Analyzed by Mercury Porosimetry in Sintered Ore

In phase analysis of sintered iron ore, pores are often considered one of the phases since it may affect sinter properties similarly with other phases. To investigate the effect of alumina on porosity, the pore structure of each sintered ore was analyzed employing Mercury Porosimetry (Quantachrome, PM-22-15). The results on sintered Carajas mix, Yandi mix, and API mix are shown in Fig. 12a–c, respectively.

Since calcium ferrite phase were shown to strongly affect the fluidity of primary melt in sintered ore [10], it was expected that the trend of sintered ore porosity will be related to the amount of SFCA-I phase previously quantified. However, such a relationship was observed only in the porosimetry of sintered Yandi ore shown by comparing Fig. 7b with Fig. 12b. Meanwhile, for the porosity trend of sintered Carajas and API ores, there was no clear relationship between porosity and alumina content or quantified SFCA-I amount. Further experiments were done using the Scanning Electron Microscopy to understand the microstructure with the increase in alumina content.

Changes in Sinter Microstructure with Alumina Addition

Change in chemical composition of sintered iron ore can affect both phase development and microstructure of the

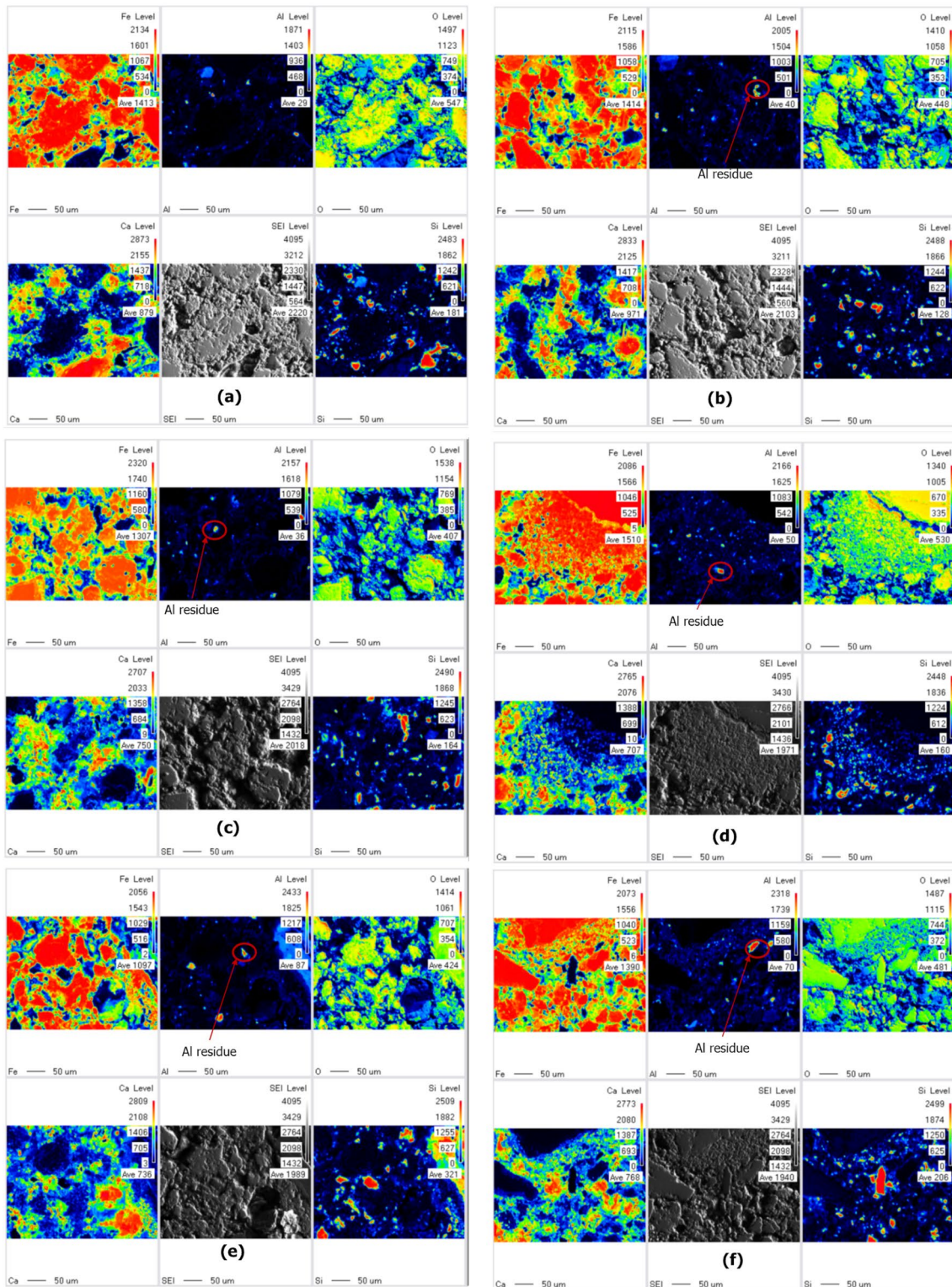


Fig. 9 Elemental mapping of sintered Carajas mix with the increase in alumina content (Wt Pct): **a** 1.40, **b** 1.82, **c** 2.24, **d** 2.66, **e** 3.51, and **f** 4.35

phases itself. Microstructures of each sintered iron ore were analyzed using Scanning Electron Microscopy, SEM (Joel-(Japan)/JSM-7100F) at an acceleration voltage of 20 keV

and magnification of 1000X. SEM image of sintered Carajas mix, Yandi mix, and API mix are shown in Figs. 13, 14, and 15, respectively.

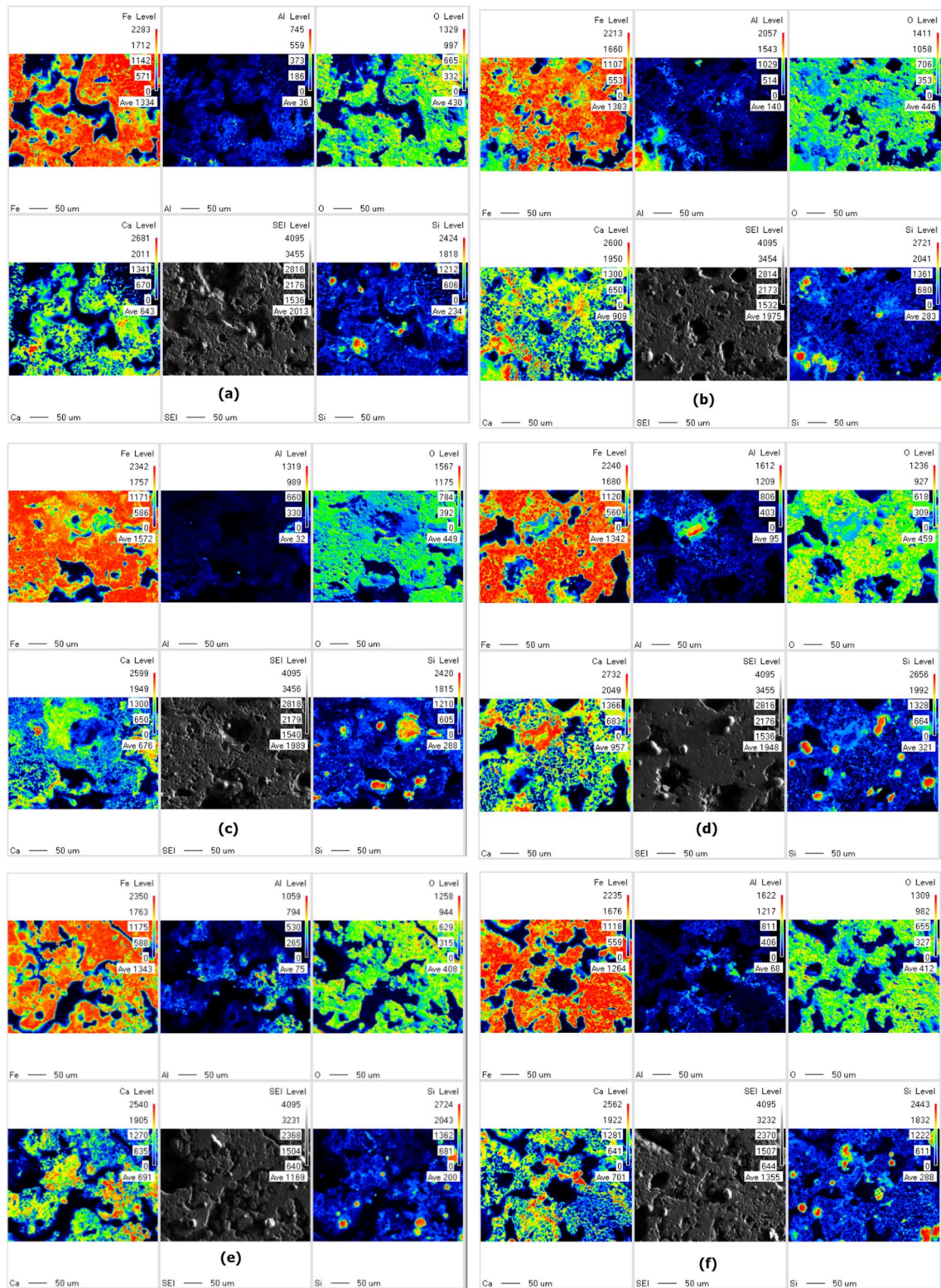


Fig. 10 Elemental mapping of sintered Yandi mix with the increase in alumina content (Wt Pct): a 1.38, b 1.80, c 2.22, d 2.64, e 3.49, and f 4.34

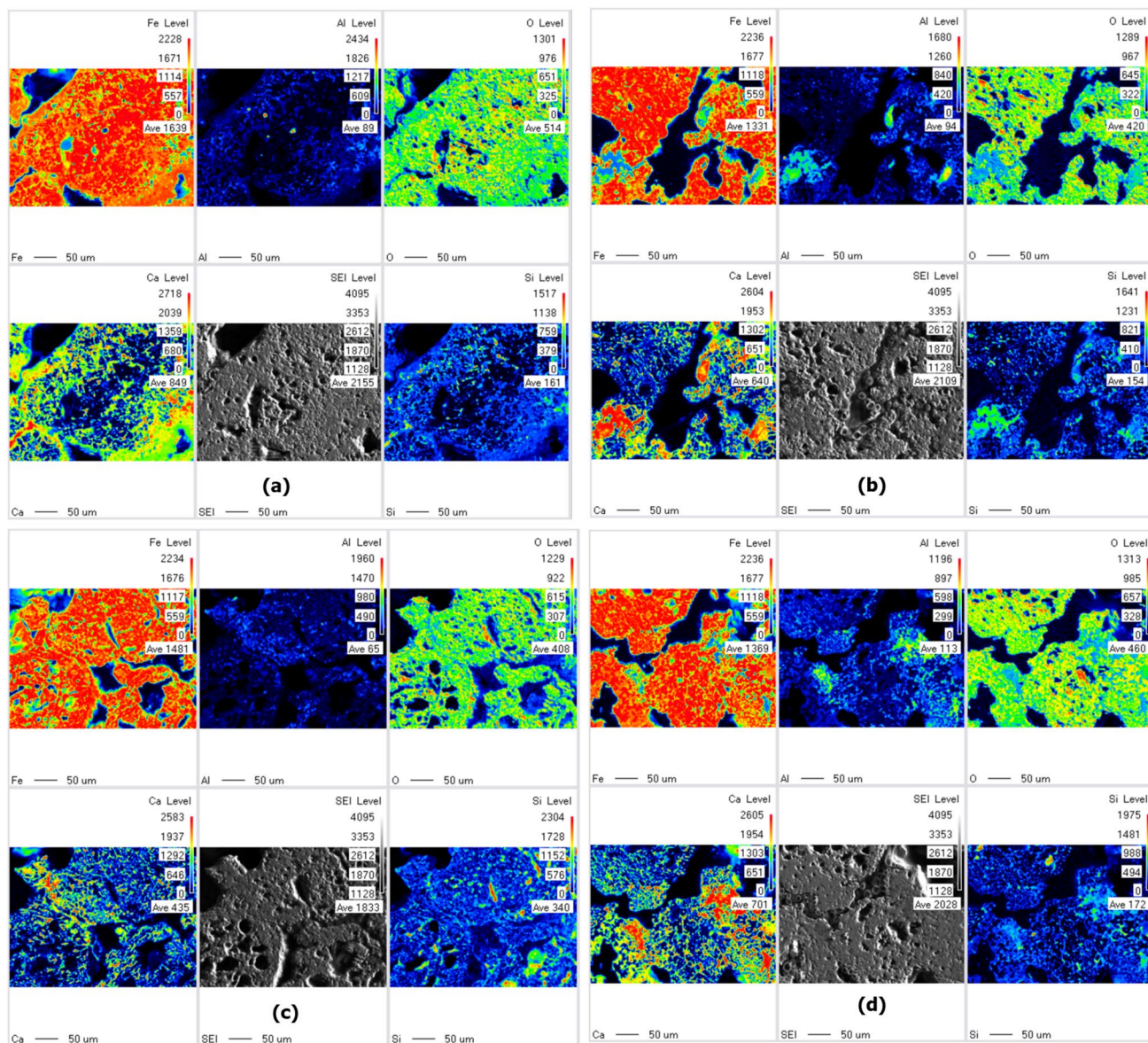


Fig. 11 Elemental mapping of sintered API mix with the increase in alumina content (Wt Pct): **a** 2.68, **b** 3.10, **c** 3.52, and **d** 4.36

As observed from Figs. 13 and 15, solid phases and pore microstructure gradually enlarge with alumina addition on sintered Carajas and API ore, which was expected to occur based on the previous studies on sinter microstructure with the increase in alumina content [16]. Meanwhile, as observed from Fig. 14 on the sintered Yandi mix, almost no significant change in microstructure was observed with the increase in alumina content.

Physical Properties of Sintered Ore

Physical properties of sintered iron ores are commonly analyzed by measuring Tumbler Index and Reduction Degradation Index. Lab scale Tumbler tests and Reduction

Degradation tests were carried out to measure Tumbler Index and RDI value of each sample for comparison purposes. However, more research is required to come up with standards to measure the lab scale physical properties results by comparing them with those obtained from the actual sintering process. Tumbler index and RDI tests were carried out using a lab scale tumbling test apparatus (Universal ball mill (JISICO J-BMM)). About 10×1 g discs were used for each tumbler and RDI tests inside a steel cylinder ($5 \text{ cm ID} \times 13.5 \text{ cm Height}$). Sintered discs were used for the tumbler test where all of the samples were revolved for 200 revolutions, while pre-reduced discs were used for RDI test where all of the samples were revolved for 200, 400, and 800 revolutions.

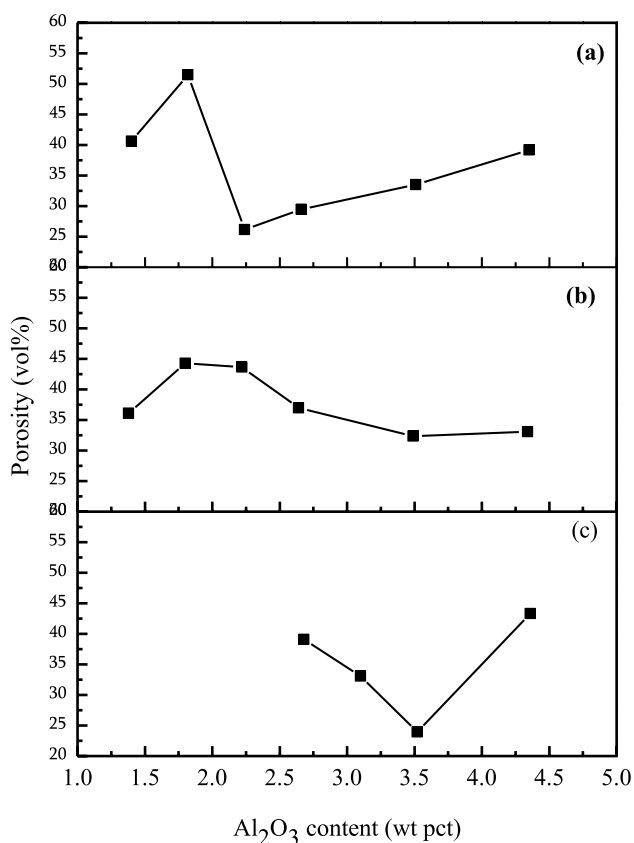


Fig. 12 Change in porosity with the increase in alumina content of a sintered Carajas mix, b sintered Yandi mix, and c sintered API mix

The results of physical properties test for sintered Carajas mix, Yandi mix, and API mix are shown in Figs. 16, 17, and 18 respectively.

As observed from Figs. 16, 17, and 18 each ore showed a different trend on physical properties with the increase in alumina content, either on tumbler index or RDI. However, as observed on Figs. 16a, 17a, and 18a, the changes in tumbler index on all samples were very small (less than 0.4 pct) and might still be inside the margin of error of measurements, therefore, for the subsequent analysis on physical properties only RDI values were considered. It should be noted that the RDI results obtained in this experiment were higher than those observed in the large scale sintering experiments, and hence these results were used for comparison purposes only to understand the relationship between phases generated, microstructure, and physical properties. More research was suggested to develop standardized lab scale physical properties test so that we can easily compare the lab scale results to those from real sinter.

Factors Governing Physical Properties of Sintered Ore

Analyses on factors governing physical properties of sintered ore were done by comparing all of the previous analyses results of the sintered iron ore mixes with the physical properties. By comparing Figs. 7a, 12a, and 16b, a certain trend on sintered Carajas ore was observed. The main features

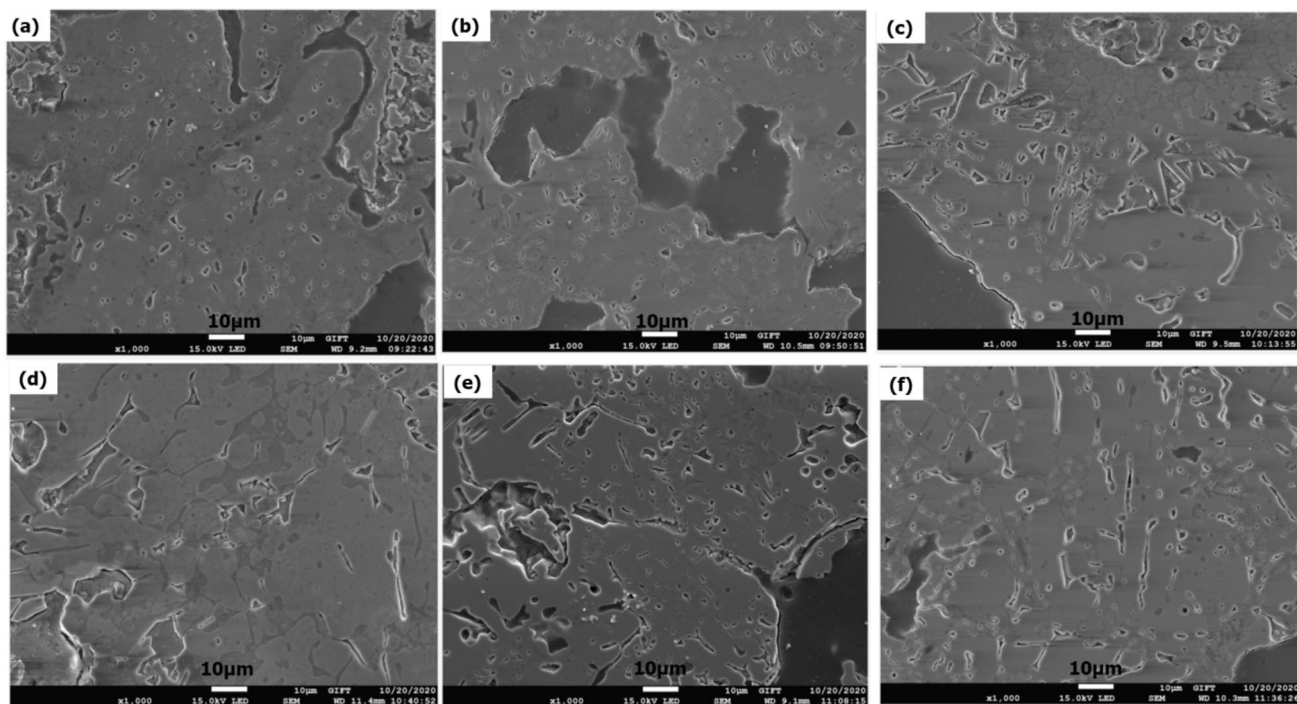


Fig. 13 SEM images of sintered Carajas mix with the increase in alumina content (Wt Pct): a 1.40, b 1.82, c 2.24, d 2.66, e 3.51, and f 4.35

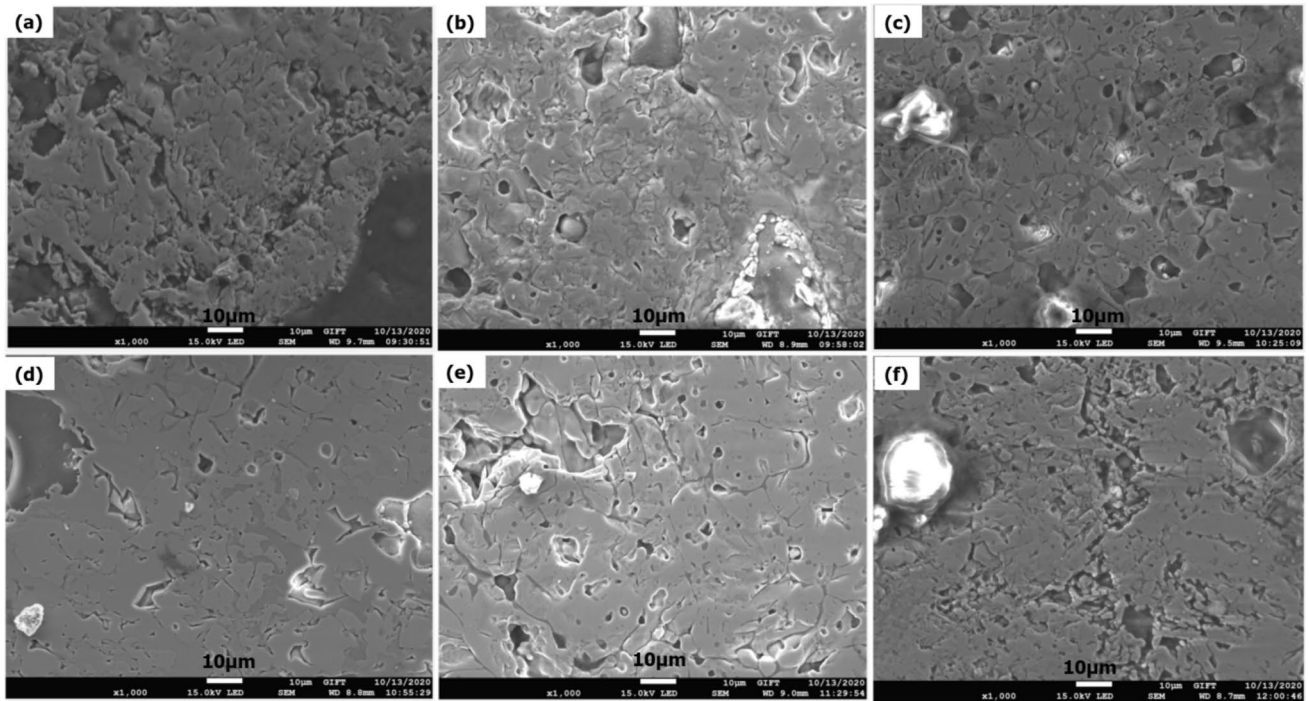
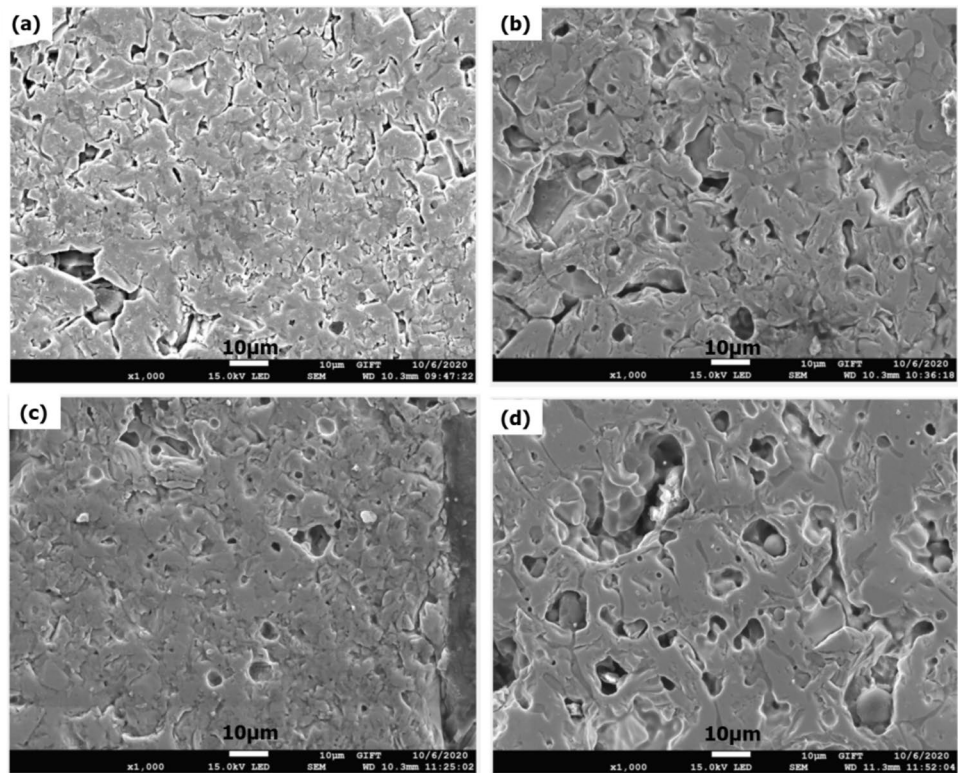


Fig. 14 SEM images of sintered Yandi mix with the increase in alumina content (Wt Pct): **a** 1.38, **b** 1.80, **c** 2.22, **d** 2.64, **e** 3.49, and **f** 4.34

Fig. 15 SEM images of sintered API mix with the increase in alumina content (Wt Pct): **a** 2.68, **b** 3.10, **c** 3.52, and **d** 4.36



which can be observed on Fig. 16b are a large drop on RDI which occurred at 1.82 wt pct alumina content and the increase in RDI trend between 2.68 wt pct and 3.52 wt pct

alumina. From Fig. 12a it can be observed that at 1.82 wt pct alumina content, a significant increase in porosity occurred, meanwhile from Fig. 7a it can be observed that between 2.68

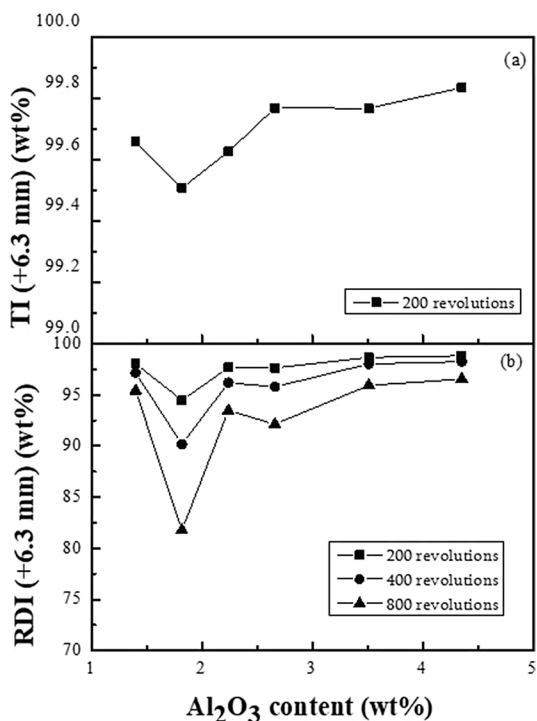


Fig. 16 Physical properties of sintered Carajas mix with the increase in alumina content: a tumbler index and b reduction degradation index

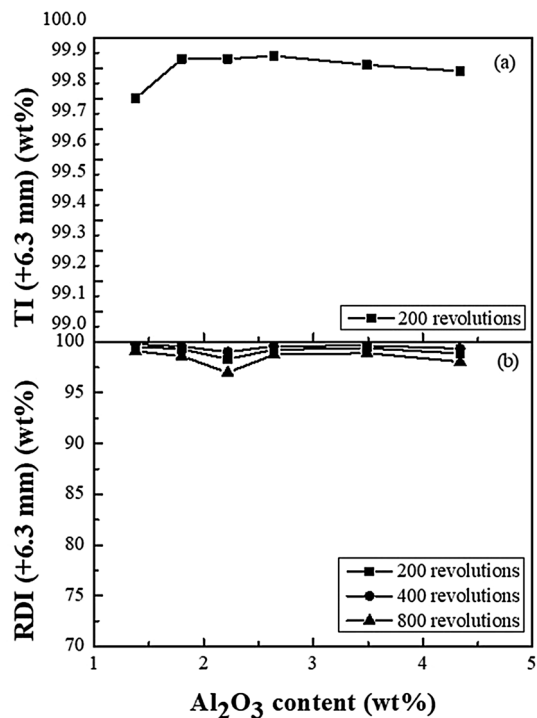


Fig. 17 Physical properties of sintered Yandi mix with the increase in alumina content: a tumbler index and b reduction degradation index

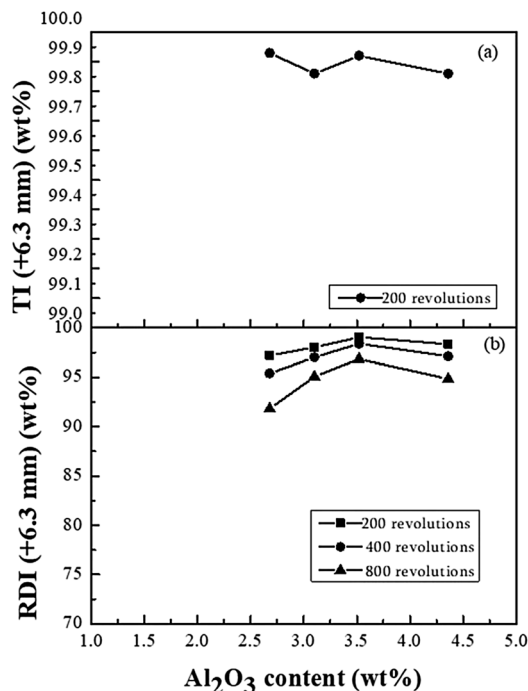


Fig. 18 Physical properties of sintered API mix with the increase in alumina content: a tumbler index and b reduction degradation index

wt pct and 3.52 wt pct alumina content, amount of SFCA phase steadily increases in similar fashion with RDI value. It seems that when total amount of SFCA phases is low, porosity has stronger effect on the physical properties of sintered ore. As amount of SFCA phases increases with more alumina addition effect of porosity become weaker and RDI value is affected by phase composition especially amount of SFCA phases. During analysis of the results of sintered API ore by comparing Figs. 7c, 12c, and 18b it seems that it follows similar relationship between phase composition, porosity, and RDI values of Carajas mix on sintered API mix with up to 4.36 wt pct alumina content. A slight decrease in RDI was observed with about 4.36 wt pct alumina content in Fig. 17b which might have been as a result of the increased porosity shown in Fig. 12c even though SFCA content increased as is shown in Fig. 7c. Based on the SEM images shown in Fig. 15 it can be observed that the sintered API mix pore sizes were greatly enlarged with the increase in alumina addition. Based on this observation it can be concluded that enlarged pore size counteracts the strengthening effect of SFCA phases which resulted in RDI deterioration even when the amount of SFCA phases are high.

As for sintered Yandi mix, observed by comparing Figs. 7b, 12b, and 17b it seemed that RDI value was also closely related to phase composition and porosity. An increase in porosity in the sintered Yandi mix shown in Fig. 12b resulted in a decrease in RDI as is shown in Fig. 17b even though SFCA amount was high with up to about 2.22

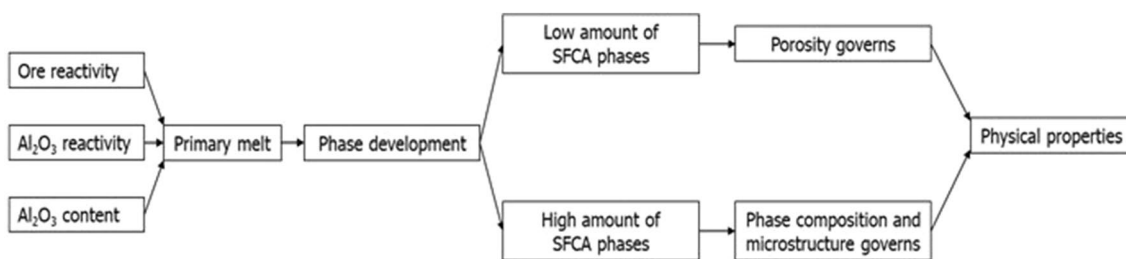


Fig. 19 Summary of factors governing physical properties of sinter with the increase in alumina content

wt pct alumina content shown in Fig. 7b. A decrease in porosity showed an increase in RDI, further increase in alumina content of up to 4.34 wt pct alumina slightly decreased RDI due to the decreased amount of SFCA even though porosity was low and not changing. Based on the results, the factors governing the sinter physical properties can be summarized as shown in Fig. 19.

Conclusions

The effect of alumina on the sinters of three kinds of iron ores such as Carajas, Yandi, and API ores was investigated to understand the correlations among the formation temperature of primary melt, calcium ferrites composition, and porosity of each sintered iron ore. From the findings, the following conclusions were obtained.

1. The estimated temperature of initial primary melt formation decreased with the addition of small amount of alumina then increased with the further addition of alumina in Yandi ore, while in Carajas and API ores was always increasing with the addition of alumina. There was a close relationship between melt formation temperature, amount of calcium ferrites, and porosity in sintered Yandi ore.
2. The total calcium ferrites phase formed increased with increase in alumina addition in sintered Carajas and API ores, while the total amount of calcium ferrites increased with the addition of small alumina, and decreased with the further addition of alumina in the sintered Yandi ore.
3. More amount of calcium ferrites were formed in the Yandi and API ores sinter than in the Carajas ore sinter, which showed that the Yandi and API ores have better reactivity since they are goethite-based ores.
4. With the increase in alumina content in the sintered iron ores, the porosity and phase composition were competing factors that may govern the physical properties of the sinter. However, the change in physical properties with the increase in alumina should be investigated in these ores.

Declarations

Conflict of interest The authors declare that they have no conflict of interest.

References

1. Mobtaker MM, Osanloo M (2015) The Southern African Institute of Mining and Metallurgy-Smart Innovation in Mining 353–364
2. Lu L, Holmes RJ, Manuel JR (2017) Effects of alumina on sintering performance of hematite iron ores. *ISIJ Int* 47(3):349–358
3. Umadevi T, Deodar AV, Mahapatra PC, Prabhu M, Ranjan M (2009) Influence of alumina on iron ore sinter properties and productivity in the conventional and selective granulation sintering process. *Steel Res Int* 80(9):686–692
4. Sinha M, Nistala SH, Chandra S, Mankhand TR (2017) Thermodynamic study of evolution of sinter phases at different alumina level. *Ironmak Steelmak* 44(2):92–99
5. Webster AS, Pownceby MI, Madsen IC, Kimpton, JA (2012) Silico-ferrite of calcium and aluminium (SFCA) iron ore sinter bonding phases: new insight into their formation during heating and cooling. *Metall Mater Trans B* 43:1344–1357
6. Liao F, Guo XM (2009) Effects of Al_2O_3 and SiO_2 on the formation process of silico-ferrite of calcium and aluminium (SFCA) by solid-state reaction. *Minerals* 9(2):101. <https://doi.org/10.3390/min9020101>
7. Scarlett NVY, Madsen IC, Pownceby MI, Christensen AN (2004) In situ X-ray diffraction analysis of iron ore sinter phases. *J Appl Cryst* 37:362–368
8. Higuchi K, Naito M, Nakano M, Takamoto Y (2004) Optimization of chemical composition and microstructure of iron ore sinter for low-temperature drip of molten iron with high permeability. *ISIJ Int* 44(12):2057–2066
9. Machida S, Nushiro K, Ichikawa K, Noda H, Sakai H (2005) Experimental evaluation of chemical composition of viscosity of melt during iron ore sintering. *ISIJ Int* 45(4):513–521
10. Okazaki J, Higuchi K, Hosotani Y, Shinagawa K (2003) Influence of iron ore characteristics on penetration behaviour of melt into ore layer. *ISIJ Int* 43(9):1384–1392
11. Loo CE, Leung W (2003) Factors influencing the bonding phase structure of iron ore sinters. *ISIJ Int* 43(9):1393–1402
12. Ji Z, Zhao Y, Gan M, Fan X, Chen X, Hu L (2019) Microstructure and minerals evolution of iron ore sinter: Influence of SiO_2 and Al_2O_3 . *Minerals* 9(7):449. <https://doi.org/10.3390/min9070449>

13. Sinha M, Nistala SH, Chandra S, Mankhand TR, Ghose AK (2017) Correlation mechanism properties of sinter phases with their chemistry and its effect on sinter quality. *Ironmak Steelmak* 44(2):100–107
14. Sinha M, Ramna RV (2009) Effect of variation of alumina on the microhardness of iron ore sinter phases. *ISIJ Int* 49(5):719–721
15. Webster AS, O’Dea DP, Ellis BG, Pownceby MI (2017) Effects of gibbsite, kaolinite and Al-rich goethite as alumina sources on silico-ferrite of calcium and aluminium (SFCA) and SFCA-I iron ore sinter bonding phase formation. *ISIJ Int* 57(1):41–47
16. Zhu D, Xue Y, Pan J, Yang C, Guo Z, Tian H, Wang D, Shi Y (2020) An investigation into alumina occurrence impact on SFCA formation and sinter matrix strength. *JMR&T* 9:10223–10234
17. Chiwandika EK, Jung S-M (2020) Effect of ilmenite ore on phase development of hematite ore sinter. *Metall Mater Trans B* 51:1469–1484
18. Hsieh L-H, Whiteman JA (1989) Sintering conditions for simulating the formation of mineral phases in industrial iron ore sinter. *ISIJ Int* 29(1):24–32
19. Webster NAS, Churchill JG, Tufaile F, Pownceby MI, Manuel JR, Kimpton JA (2016) Fundamentals of silico ferrite of calcium and aluminium (SFCA) and SFCA-I iron ore sinter bonding phase formation: effects of titanomagnetite-based ironsand and titanium addition. *ISIJ Int* 56(10):1715–1722
20. Nicol S, Chen J, Pownceby MI, Webster NAS (2018) A review of the chemistry, structure and formation condition of silico-ferrite of calcium and aluminium (SFCA) phases. *ISIJ Int* 58(12):2157–2172
21. Guo H, Guo XM (2019) Effect of alumina on liquid phase formation in sintering process of iron ore fines. *Steel Res Int* 90:1900138. <https://doi.org/10.1002/srin.201900138>

Publisher’s Note Springer Nature remains neutral with regard to jurisdictional claims in published maps and institutional affiliations.